Preprint: EXP - S

MULTI-SCALE INTERACTION NEAR LOCKED MAGNETIC ISLANDS AND RESULTING DISRUPTION DELAY IN KSTAR

¹J. KIM, ²G.J. CHOI, ³M.K. JUNG, ¹M.J. CHOI, ¹J. LEE, ¹J.W. JUHN, ¹J.M. KWON, ³Y.S. NA

¹Korea Institute of Fusion Energy, Daejeon, Republic of Korea

Email: jayhyunkim@kfe.re.kr

Abstract

Understanding the factors that drive disruption dynamics and advancing their control are critical for realizing fusion reactor development. In magnetic fusion devices, plasma disruptions often result from disturbances in magnetic field structures caused by phenomena such as the growth of magnetic islands. Notably, even seemingly identical magnetic islands can display significantly different disruption behaviours depending on the surrounding turbulence levels. Weaker turbulence requires stronger magnetic island drivers to trigger disruptions, potentially delaying their onset. This study investigates the controlled manipulation of macro-scale plasma disruptions by modulating micro-scale turbulence through meso-scale poloidal flows, using additional n=2 non-axisymmetric (NA) magnetic field perturbations in KSTAR discharges. Furthermore, GENE gyrokinetic simulations, replicating these discharges, yield results that qualitatively align with experimental observations. Intriguingly, GENE simulations reveal a reduction in outward heat flux near the q=2 surface, where the 2/1 magnetic island is located, due to the presence of a 3/2 island at q=3/2 surface. Further simulations exploring the nonlocal characteristics of multiscale interactions among micro-scale turbulence, meso-scale flows, and macro-scale NA magnetic field perturbations, as well as the conditions for disruption control based on these interactions, will be presented.

1. INTRODUCTION

Magnetic fusion devices such as tokamaks and stellarators maintain their confinement due to nested flux surfaces formed by precisely controlled magnetic fields. However, plasma instabilities (e.g., neo-classical tearing modes) or external perturbation of magnetic fields (e.g., error fields) can disturb these nested flux surfaces by inducing macro-scale structures such as magnetic islands. In severe cases, such disturbances degrade confinement performance or, if sufficiently intense, lead to plasma disruption, resulting in the complete loss of confinement.

The disturbances of nested flux surfaces occur via magnetic reconnection, leading to the formation of stochastic field lines or cold bubbles [1]. While macro-scale phenomenon, such as the destruction of nested flux surfaces, is driven by magnetic reconnection, the reconnection process itself is strongly influenced by micro-scale physics, such as plasma resistivity. Consequently, modifying the magnetic reconnection process through various mechanisms, including multi-scale interactions, can, in turn, impact macro-scale plasma disruptions.

Although the ultimate goal of this study is to control disruption by influencing the micro-scale physics that governs the disruption process, the actuation employed for this purpose was applied at the macro-scale as well. Specifically, in this work, an additional NA field with a different toroidal mode number, n=2, was applied. In general, tokamak devices demand an almost perfect level of symmetry (<10⁻⁴ order) to achieve high confinement and stability. Therefore, the fact that an n=2 NA field—which introduces additional symmetry breaking on the system—can delay a major disruption, may at first glance appear to be a paradoxical result. To explain the effects of additional symmetry breaking that are difficult to understand on the macro-scale, it is necessary to examine the interactions across multi-scales.

A key distinction to note is that, in conventional discussions of disruption avoidance in magnetic fusion devices, the focus is on preventing disruption by directly controlling the macro-scale disturbances (e.g., MHD instabilities) that cause plasma disruption. To this end, typical approaches include applying correction fields to counteract error fields (EFs), ideally by generating an opposing field, or compensating the perturbed bootstrap current through electron cyclotron current drive. In contrast, this study addresses cases where direct control of the disturbance itself is not feasible, and thus disruption avoidance is unattainable. The objective is to regulate the dynamics of the disruption process, thereby extending the response time available for a disruption mitigation system or enhancing the overall efficiency of disruption mitigation.

This manuscript outlines the experimental method in Section 2 and presents the experimental results in Section 3. In particular, Section 3 begins by mentioning the possible influence of the intrinsic EF on experimental condition

²Korea Advanced Institute of Science and Technology, Daejeon, Republic of Korea

³Seoul National University, Seoul, Republic of Korea

control, in order to distinguish it from the usual disruption avoidance achieved through EF correction. Building on this, we then investigate the effect of the n=2 NA field—used as an actuator of multi-scale interaction—on disruption dynamics. In Section 4, these results are incorporated into a global gyro-kinetic simulation, which computationally reproduces the experimental results. Section 5 is wrapped up with discussion and summary.

2. EXPERIMENTAL METHOD

As illustrated in Fig. 1, KSTAR is equipped with three pairs of picture frame coils—designated as top, middle, and bottom field error correction (FEC) coils—arranged in the poloidal direction [2]. Such FEC coils can, conversely, also be used to apply an additional error field, and in this experiment, they were utilized for that purpose. Each FEC coil is toroidally segmented into four parts, limiting the maximum applicable toroidal mode number (n) of the NA field to two. The parity of each picture frame coil, defined by the outward (+) or inward (-) radial direction of the generated field, determines the resulting toroidal mode number and phase of the NA field through the combination of coil parities. Similarly, the relative toroidal phases of the top, middle, and bottom FEC coils govern the poloidal phasing, i.e., the pitch of the resulting NA field relative to the equilibrium field.

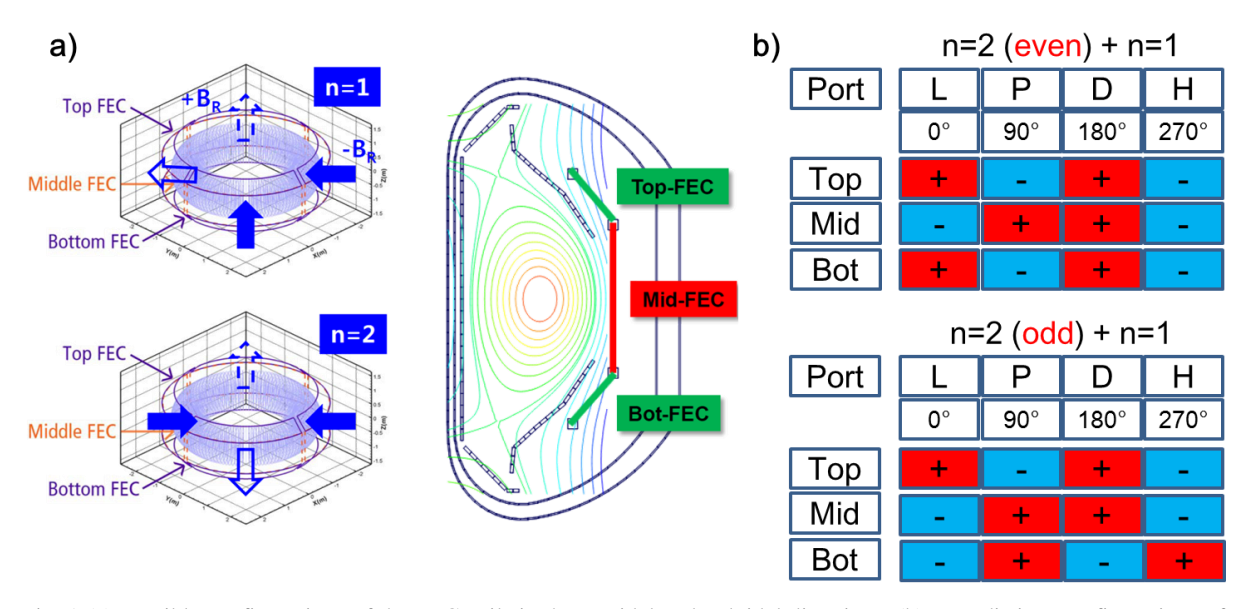


Fig. 1 (a) Possible configurations of the FEC coils in the toroidal and poloidal directions. (b) Two distinct configurations of the n=2 NA field from the top and bottom FEC coils combined with the n=1 NA field from the middle FEC coil: specifically, the n=2 even and odd configurations.

The n=2 even configuration of the top and bottom FEC coils was employed to apply an n=2 NA field, alongside the n=1 proxy EF from the middle FEC coils. The term "proxy EF" specifically denotes an NA field that induces plasma locking and disruption. Due to the four-fold coil structure, the n=1 EF applied through the mid-FEC coil can rotate continuously in the toroidal direction. However, the n=2 NA field cannot rotate continuously and can only undergo a sign flip. In this study, the L-port of KSTAR, among its total 16 ports, which serves as the reference for the toroidal phase, was set as toroidal phase 0° . Based on this reference, the outward normal direction of each NA field was defined in the counter-clockwise direction seeing from the top view. Consequently, for the n=2 NA field, only two applications are possible: at toroidal phases 0° and 90° .

An NB-heated L-mode discharge was used as the target discharge. The rationale for selecting L-mode instead of H-mode is as follows. When the magnetic island grows large enough to cause locking and disruption, an H-L back transition typically occurs before disruption, causing the actual major disruption to take place in the locked L-mode state. To eliminate uncertainties in quantification caused by uncontrolled changes during the H-L back transition, the target discharge was chosen as an L-mode discharge. In particular, mode locking is highly sensitive to plasma density, and the abrupt density drop associated with the H-L back transition can significantly affect the quantification of disruption dynamics.

Density feedback control was employed to maintain a consistent density level across the comparative shots. Furthermore, the electron temperature and thermal energy were kept comparable prior to the onset of mode locking. However, owing to rapid variations such as minor disruptions occurring after locking, it was not possible to

preserve fully identical shot conditions through density feedback alone. Nevertheless, the influence of the n=2 NA fields could be reliably assessed from the systematic tendencies observed over a series of experiments.

In the experiments conducted prior to 2023, a lower single-null (LSN) configuration with a favourable ∇B direction was employed. In 2024, to avoid the effects of tungsten impurities originating from the tungsten divertor installed at the bottom of the vacuum vessel in 2023, the experiments were carried out using an upper single-null (USN) configuration. In Fig. 2, the LSN configuration and the lower divertor used prior to 2023 are shown in black, while the USN configuration and the new tungsten lower divertor used after 2023 are shown in purple. In both plasma configurations, the application of an additional n=2 NA field was found to delay the major disruption.

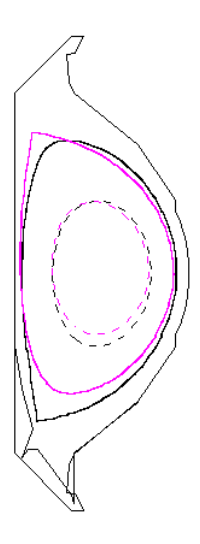


Fig. 2 Configuration of target discharges before and after tungsten divertor installation.

For a detailed experimental analysis, it is necessary to measure magnetic islands, poloidal flow, and turbulence—which are involved in multi-scale interactions—with sufficient spatiotemporal resolution. Using the electron cyclotron emission imaging (ECEI) system installed on KSTAR, combined with a high-sampling digitizer, various physical phenomena occurring at multi-scales were simultaneously measured.

3. EXPERIMENTAL RESULT

3.1. Macro-scale observation in experiments

The gradual increase in the n=1 proxy EF on the target discharge, which originally had no pre-existing MHD instabilities, led to the formation of a locked magnetic island and ultimately resulted in major plasma disruption. Figure 3 presents two discharges illustrating the disruption delay depending on the presence or absence of the additional n=2 NA field. In the case of shot #37111, where an additional n=2 NA field was generated by driving a 2 kA/turn current through the top and bottom coils, a major disruption did not occur despite the application of the maximum n=1 NA field achievable in KSTAR. It was only after the n=2 NA field was turned off that a major disruption was triggered by the n=1 NA field. However, in the case of shot #37110, a major disruption occurred before the n=1 NA field reached its maximum, and the discharge ended at t=7.17 seconds with major disruption.

In the case of shot #37111, as compared with #37110, it is noteworthy that, as shown in Fig. 3(c), locking occurred about 0.59 seconds earlier due to the additional n=2 NA field. Non-axisymmetric fields reduce rotation through mechanisms such as neoclassical toroidal viscosity, and the extra rotation drop induced by the n=2 NA field led to the earlier locking observed in #37111. This provides evidence that the externally applied n=2 NA field in #37111 did not act to cancel the intrinsic n=2 EF. If the external n=2 NA field had indeed cancelled the intrinsic n=2 EF, then locking in #37111 should have been delayed compared to #37110. It should also be emphasized here that the physical mechanism governing the loss of torque balance leading to locking is different from that driving magnetic reconnection, which causes disruption.

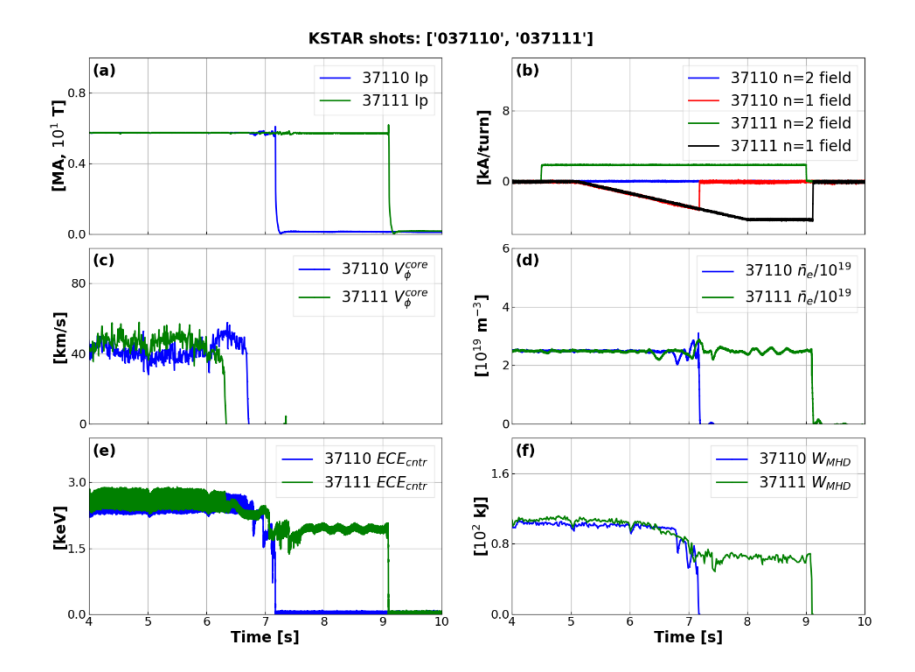


Fig. 3. Delay of plasma disruption due to additional n=2 NA fields: Comparison between shot 37110 (without n=2 NA fields) and shot 37111 (with n=2 NA fields). In both shots, the n=1 field is applied in the same manner up to its maximum. (a) Plasma current, (b) NA field coil currents, (c) toroidal rotation, (d) plasma density, (e) electron temperature, and (f) stored energy.

3.2. Multi-scale phenomena in disruption dynamics

During this process, as the plasma approached disruption, strong turbulence was observed near the x-point of the locked magnetic island. Previous studies in both magnetic fusion and astrophysical plasmas have reported that turbulence can accelerate magnetic reconnection [3, 4]. Building on this, we hypothesized that suppressing turbulence—thereby reducing turbulence-driven hyper-resistivity—could impede reconnection and delay disruption. To test this, a comparative experiment was conducted as described in Subsection 3.1, where an external n=2 perturbed magnetic field was additionally applied to the same discharge to drive poloidal flow around the n=1 locked magnetic island.

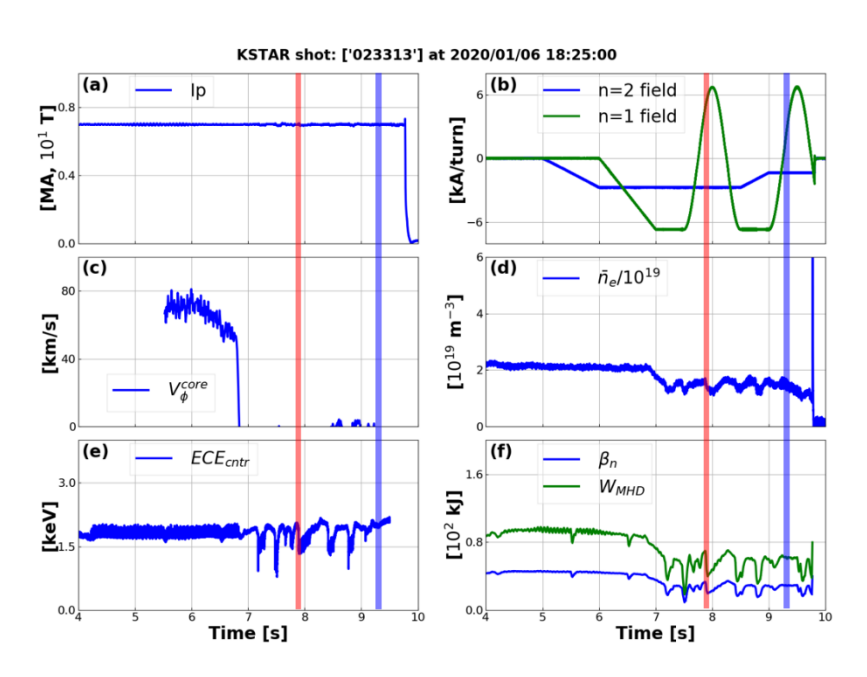


Fig. 4. (a) Plasma current, (b) NA field coil currents, (c) toroidal rotation, (d) plasma density, (e) electron temperature, and (f) stored energy.

In discharge #23313 shown in Fig. 4, the n = 1 field was rotated by 360° at two different levels of the n = 2 NA field to observe changes in the overall turbulence around the magnetic island. As a result, as shown in Fig. 5, the flow and flow shear surrounding the magnetic island were experimentally confirmed to increase in proportion to the n = 2 NA field level.

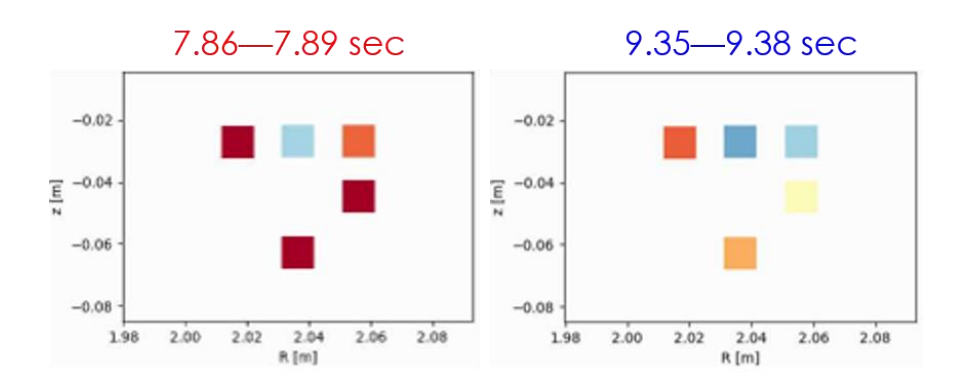


Fig. 5. Poloidal flows near the 2/1 magnetic island, with each time window shown in Fig. 4.

Diagnostic analyses further revealed that the coexistence of 2/1 and 3/2 islands enhanced poloidal shear flow, which in turn correlated with reduced fluctuation amplitudes. These findings suggest that magnetic islands interact with micro-scale turbulence through self-generated flows, consistent with earlier experimental [5], numerical [3–5], and analytical studies [6, 7]. Moreover, experimental observations indicated that turbulence around the x-point was mitigated by the meso-scale poloidal flow [5].

4. NUMERICAL SIMULATION

Global nonlinear gyrokinetic simulations were performed using the GENE code [10-11], which has previously been used extensively to study multi-scale interaction involving magnetic islands [12-14].

4.1. Simulation setup

We performed δf electrostatic gyrokinetic simulations, treating both ions and electrons gyro-kinetically, in a circular concentric magnetic geometry. Kinetic profiles fitted from KSTAR shots #23315 and #23317 were used for the double-island case (n = 1 EF and n = 2 NA fields) and the single-island case (n = 1 EF only), respectively. A detailed comparison between the experimental and fitted profiles is provided in Fig. 6.

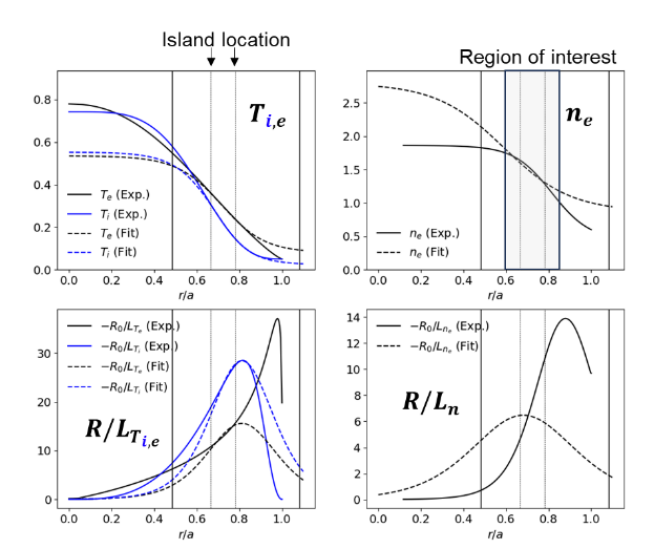


Fig. 6. Profiles used for GENE simulations.

Static magnetic islands were introduced via perturbations of the parallel vector potential δA_{\parallel} , expressed as [12,15]:

$$\delta A_{\parallel} = \frac{W^2 B_0 \hat{s}}{16 q_s R_0} e^{i k_y^I (y - \hat{s} X z)} A_x$$

Here, W is the island width, B_0 the background magnetic field, \hat{s} the magnetic shear at the resonant surface, q_s the safety factor at the resonant surface, R_0 the major radius, k_y^I the island mode number, and $X = x - x_s$ the radial coordinate. The coordinates (x,y,z) denote the radial, binormal, and parallel directions, respectively. A_x is a radial envelope used to prevent boundary interference; no radial asymmetry was introduced. Two runs were conducted to compare single- and double-island cases: only 2/1 island was involved in the single-island run, whereas 3/2 island was added in the double-island run. The widths of the 3/2 and 2/1 islands are set to be 15 ρ_s and 20 ρ_s respectively based on the ECEI diagnostics of KSTAR.

4.2. Heat flux profile

To compare transport and confinement between the single- and double-island cases, we analysed the heat flux profiles. Figure 7 presents the flux-surface-averaged ion and electron heat fluxes, normalized to the gyro-Bohm level. Overall, the double-island case exhibits reduced heat flux, indicating improved confinement. In both cases, localized dips in heat flux appear near the island locations, originating from profile flattening within the separatrix that diminishes the turbulence drive.

Another notable feature is the localized bump in heat flux just outside the island separatrix. In the single-island case, this bump is pronounced around the q=2 surface. It arises from the steepening of gradients outside the island: as the profile flattens inside, gradients sharpen immediately beyond the separatrix, enhancing turbulence drive. By contrast, this effect is far less evident in the double-island case, suggesting stronger turbulence regulation and suppressed transport despite the presence of steepened gradients.

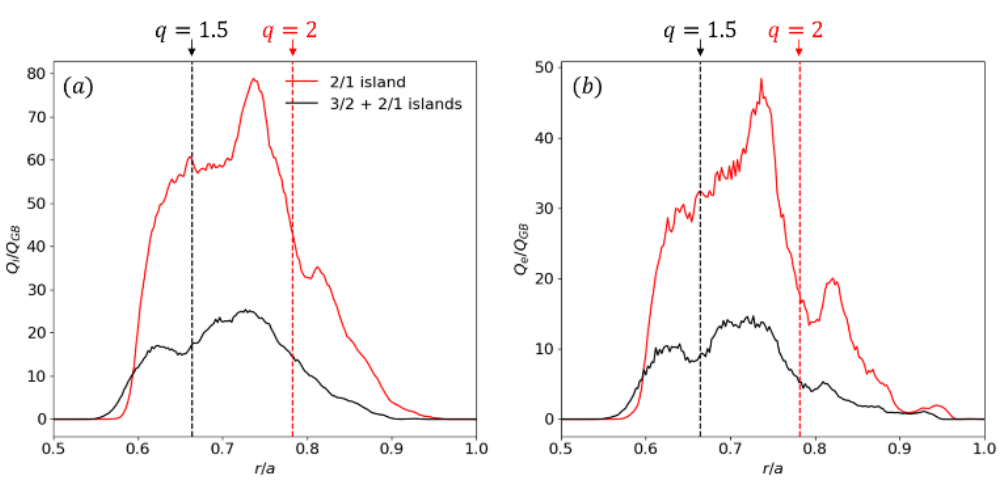


Fig. 7. Flux-surface-averaged heat flux profile comparison. (a) is ion heat flux normalized to gyro-Bohm, and (b) is the electron heat flux normalized to gyro-Bohm.

4.3. Helical shear flow profile

Magnetic islands are known to drive vortex flows, as established by theory [16–18], experiments [19–21], and simulations [12, 22–23]. These vortex flows act as shear flows that regulate turbulence in the vicinity of the island. Figure 8 compares flux-surface-averaged helical flow profiles for the single- and double-island cases, showing a clear divergence between the two scenarios. In the single-island case, the helical flow reverses direction across the q=2 surface, consistent with previous numerical [12] and experimental [19] studies of large islands. In contrast, in the double-island case, the flows remain co-directional across both islands, in agreement with prior results for smaller islands [12, 22].

As a result, the shear flow characteristics differ significantly in the region between the q = 1.5 and q = 2 surfaces. In this region, the helical flow reflects the combined influence of zonal flows and island-driven flows. The presence of the 3/2 island enhances the shear in the double-island case, which is likely responsible for the suppression of the heat flux bumps described above.

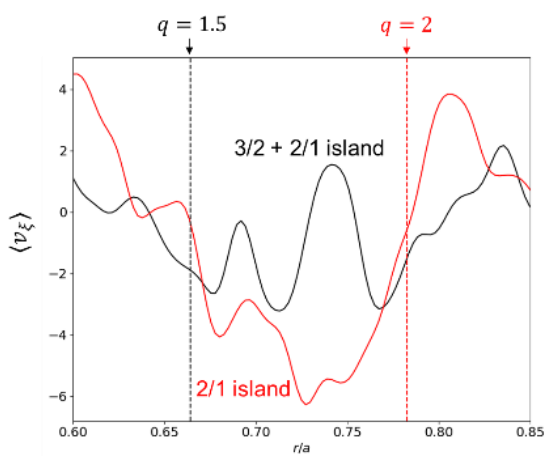


Fig. 8. Flux-surface-averaged helical flow profile.

5. DISCUSSION AND SUMMARY

This study was initiated to explain disruption delays in tokamaks by additional symmetry breaking fields, where such delays could not be accounted for by macro-scale physics alone. Ultimately, the phenomena observed in experiments were explained through meso-scale and micro-scale physics, which in turn determine the effective macro-scale behaviour. To achieve this, we employed both diagnostics capable of measuring meso- and micro-scale physics.

To further clarify the observed multi-scale interactions, numerical simulations were performed using the global gyrokinetic code **GENE** [10, 11] under conditions similar to those of the experiment [5]. The simulations qualitatively reproduce experimental trends, revealing complex helical flow structures generated by the interplay between 2/1 and 3/2 islands. These flows regulate both the amplitude and spatial distribution of micro-scale turbulence. Moreover, the heat flux profiles are significantly modulated by the coexistence of multiple islands and their relative phase differences.

This study demonstrates not only the feasibility of controlling plasma disruption dynamics through externally applied macro-scale control knobs but also underscores the intricate influence of micro- and meso-scale physics on macro-scale phenomena. Such findings are expected to contribute to advanced disruption control strategies and may also provide insights into magnetic reconnection in astrophysical plasmas, where multiple celestial bodies interact.

In summary, this study highlights the coupling between macro-scale magnetic islands, meso-scale flows, and micro-scale turbulence, offering new perspectives on disruption control strategies for KSTAR and for future tokamaks such as ITER. Ongoing work will focus on refining non-axisymmetric field configurations to further optimize "disruption resilience".

ACKNOWLEDGEMENTS

This research was supported by R&D Program of "High Performance Tokamak Plasma Research & Development (code No. EN2501)" through the Korea Institute of Fusion Energy (KFE) funded by the Government funds, Republic of Korea.

REFERENCES

- [1] MIRNOV S. et al., "ITER Physics Basis Chapter 3: MHD stability, operational limits and disruptions", Nucl. Fusion, **39** (1999) 2251.
- [2] KIM H.K. et al., "Design features of the KSTAR in-vessel control coils", Fusion Eng. Des., 89 (2009) 1029.
- [3] STRAUSS, H.R., "Hyper-resistivity produced by tearing mode turbulence", Phys. Fluids 29 (1986) 3668-3671.

- [4] LAZARIAN, A. et al., "3D turbulent reconnection: Theory, tests, and astrophysical implications", Phys. Plasmas 27 (2020) 012305.
- [5] KIM, J. et al., "Evolution of locked mode under the existence of NA fields", EX/P7-14 presented at IAEA fusion energy conference, Ahmedabad, 2018.
- [6] KWON J.-M. et al., "Gyrokinetic simulation study of magnetic island effects on neoclassical physics and microinstabilities in a realistic KSTAR plasma", Phys. Plasmas, **25** (2018) 052506.
- [7] POLI E. et al., "Gyrokinetic and gyrofluid investigation of magnetic islands in tokamaks", Plasma Phys. Control. Fusion, 52 (2010) 124021.
- [8] YOON E.S. et al., "Turbulence spreading induced vortex flow generation in a magnetic island", Nucl. Fusion 64 (2024) 126050.
- [9] GÖRLER, T. et al., "The global version of the gyrokinetic turbulence code GENE", Journal of Computational Physics 230 (2011) 7053.
- [10] JENKO, F., DORLAND, W., KOTSCHENREUTHER, M., Electron temperature gradient driven turbulence, Phys. Plasmas 7 5 (2000) 1904-1910.
- [11] GORLER, T., LAPILLONNE, X., BRUNNER, S., DANNERT, T., JENKO, F., MERZ, F., TOLD, D., The global version of the gyrokinetic turbulence code GENE, J. Comput. Phys. **230** 18 (2011) 7053-7071.
- [12] BANON NAVARRO, A., BARDOCZI, L., CARTER, T. A., JENKO, F., RHODES, T. L., Effect of magnetic islands on profiles, flows, turbulence and transport in nonlinear gyrokinetic simulations, Plasma Phys. Control. Fusion 59 3 (2017) 034004.
- [13] BARDOCZI, L., RHODES, T. L., BANON NAVARRO, A., SUNG, C., CARTER, T. A., LA HAYE, R. J., MCKEE, G. R., PETTY, C. C., CHRYSTAL, C., JENKO, F., Multi-field/-scale interactions of turbulence with neoclassical tearing mode magnetic islands in the DIII-D tokamak, Phys. Plasmas 24 5 (2017) 056106.
- [14] JITSUK, T., DI SIENA, A., PUESCHEL, M. J., TERRY, P. W., WIDMER, F., POLI, E., SARFF, J. S., Global linear and nonlinear gyrokinetic simulations of tearing modes, Nucl. Fusion **64** 4 (2024) 046005.
- [15] ZARZOSO, D., HORNSBY, W. A., POLI, E., CASSON, F. J., PEETERS, A. G., NASR, S., Impact of rotating magnetic islands on density profile flattening and turbulent transport, Nucl. Fusion **55** 11 (2015) 113018.
- [16] HAHM, T. S., KIM, Y. J., DIAMOND, P. H., CHOI, G. J., Anisotropic $E \times B$ shearing rate in a magnetic island, Phys. Plasmas, **28** 2 (2021) 022302.
- [17] LECONTE, M., CHO, Y. W., Turbulence-driven vortex-flow around a magnetic island, Nucl. Fusion 63 3 (2023) 034002.
- [18] CHOI, G. J., HAHM, T. S., Long term vortex flow evolution around a magnetic island in tokamaks, Phys. Rev. Lett. **128** 22 (2022) 225001.
- [19] CHOI, M. J., KIM, J., KWON, J.-M., PARK, H. K., IN, Y., LEE, W., LEE, K. D., YUN, G. S., LEE, J., KIM, M., KO, W.-H., LEE, J. H., PARK, Y. S., NA, Y.-S., LUHMANN JR, N. C., PARK, B. H., Multiscale interaction between a large scale magnetic island and small scale turbulence, Nucl. Fusion 57 12 (2017) 126058.
- [20] IDA, K., OHYABU, N., MORISAKI, T., NAGAYAMA, Y., INAGAKI, S., ITOH, K., LIANG, Y., NARIHARA, K., KOSTRIOUKOV, A. Y., PETERSON, B. J., TANAKA, K., TOKUZAWA, T. KAWAHATA, K. SUZUKI, H., KOMORI, A., Observation of plasma flow at the magnetic island in the large helical device, Phys. Rev. Lett. 88 1 (2002) 015002.
- [21] ESTRADA, T., ASCASIBAR, E., BLANCO, E., CAPPA, A., HIDALGO, C., IDA, K., LOPEZ-FRAGUAS, A., VAN MILLIGEN, B. P., Plasma flow, turbulence and magnetic islands in TJ-II, Nucl. Fusion **56** 2 (2016) 026011.
- [22] FANG, K. S., LIN, Z., Global gyrokinetic simulation of microturbulence with kinetic electrons in the presence of magnetic island in tokamak, Phys. Plasmas **26** 5 (2019) 052510.
- [23] HORNSBY, W. A., PEETERS, A. G., SNODIN, A. P., CASSON, F. J., CAMENEN, Y., SZEPESI, G., SICCINIO, M., POLI, E., The nonlinear coupling between gyroradius scale turbulence and mesoscale magnetic islands in fusion plasmas, Phys. Plasmas 17 9 (2010) 092301.